



VirtualBrainCloud

Personalized Recommendations for Neurodegenerative Disease



https://twitter.com/tvb_cloud

Public deliverable report

D3.7: FULL-COHORT INDIVIDUAL MEG BRAIN DYNAMICS MEASURES

Date November 2021

Authors Ehtasham Javed, Sheng H. Wang, Felix Siebenhühner, J. Matias Palva, Satu Palva (UNIVERSITY OF HELSINKI, UH)
Isabel Suárez, Gianluca Susi, Fernando Maestú (UNIVERSIDAD COMPLUTENSE DE MADRID, UCM)

© VirtualBrainCloud consortium

Dissemination level: **public**
Website <https://virtualbraincloud-2020.eu>



This project has received funding from the European Union's Horizon 2020 research and innovation programme under grant agreement No 826421



Contents

1. Introduction	3
1.1 Templates used for brain parcellation	3
2. Partners involved	4
3. Description of work performed	4
3.1 Individual dynamic measures	4
3.1.1 Long-range temporal correlations (LRTC)	4
3.1.2 Functional excitation-inhibition ratio (fE/I)	5
3.2 Inter-areal dynamics	5
3.2.1 Phase-locking value (PLV)	5
3.2.2 Corrected imaginary phase-locking value (ciPLV)	6
3.2.3 Weighted phase lag index (wPLI)	6
3.2.4 Amplitude envelope correlation (AEC)	8
3.2.5 Cross-frequency synchrony (CFS) and phase-amplitude coupling (PAC)	8
4. Conclusion	8



1. Introduction

The MEG full-cohort database was introduced on TVB-Cloud public **Deliverable 3.5**. This dataset provided electrophysiological, structural, genetic, demographic, and neuropsychological data pertaining to four different diagnostic categories in the Alzheimer’s disease (AD) continuum (i.e., healthy older adults (HC), older adults with subjective cognitive decline (SCD), older adults with mild cognitive impairment (MCI), and patients with AD). In **Deliverable 3.7**, we complete the full-cohort database by providing additional individual dynamic measures including local dynamics (long-range temporal correlation (LRTC), functional excitation-inhibition ratio (fE/I)), and inter-areal dynamics (functional connectomes of phase (i.e., phase-locking value (PLV), corrected imaginary phase-locking value (ciPLV), weighted phase lag index (wPLI)), amplitude coupling (amplitude envelope correlation (AEC)), cross-frequency synchrony (CFS), and phase-amplitude coupling (PAC). All the measures were anatomically parceled into sets of regions of interest (ROIs) following commonly used templates (e.g., Schaefer (SCH), Automated Anatomical Labeling (AAL), and Harvard-Oxford (HO)) (see **Table 2**). Access to the full-cohort measures will be granted after approval of request, which should be sent to IPs fernando.maestu@ctb.upm.es (CC: gianluca.susi@ctb.upm.es and isabel.suarez@ctb.upm.es) and for dynamic brain measures calculated at UH, send email to satu.palva@helsinki.fi and/or matias.palva@helsinki.fi.

Table 1. Summary description for the MEG full-cohort database. HC: healthy controls; SCD: subjective cognitive decline; MCI: mild cognitive impairment; AD: Alzheimer’s disease.

	HC	SCD	MCI	AD
N	119	88	142	15
Gender (females)	79	70	93	7
Age (years)	70.29 ± 4.38	72.34 ± 5.21	73.40 ± 5.44	76.73 ± 5.20
MEG	119	88	142	15
T1-MRI	119	88	142	15
dw-MRI	107	80	122	11

1.1 Templates used for brain parcellation

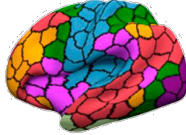
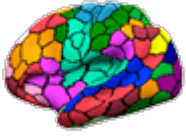
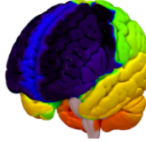
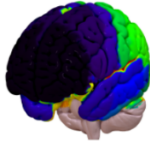
The dimensionality of the acquired brain data can be conveniently reduced by collapsing channels or reconstructed sources to a brain atlas, comprising some dozens or hundreds of brain regions (often also called “parcels”). Brain atlases play a key role in modern neuroimaging analysis of brain structure and function, allowing the comparability of the results across subjects, the improvement of the signal-to-noise ratio, and importantly, the reduction of the size of the data.

The impact of the different brain parcellations on the structural and functional brain connectomes has been one of the objects of study of **Task 3**, formalized in **Deliverable 3.9**. With the aim of harmonizing the



different outputs of the project, here we consider the **Schaefer** (SCH) (Schaefer et al., 2018) as the main parcellation template. All the indices are extracted using this atlas. Additionally, some indices are provided in different atlases used in previous deliverables, i.e., the AAL (Tzourio-Mazoyer et al., 2002) and HO (Desikan et al., 2006; Frazier et al., 2005; Goldstein et al., 2007; Makris et al., 2006) atlases.

Table 2. Summary of the brain atlases used in the deliverable.

Brain parcellation	Number of ROIs	Presentation	Reference
Schaefer (SCH)	100 (17 networks)		(Schaefer et al., 2018)
	400 (17 networks)		
Automated Anatomical Labeling (AAL)	90		(Tzourio-Mazoyer et al., 2002)
Harvard-Oxford (HO)	64		(Desikan et al., 2006; Frazier et al., 2005; Goldstein et al., 2007; Makris et al., 2006)

2. Partners involved

- University of Helsinki (UH) – *Lead*.
- Complutense University of Madrid (UCM).

3. Description of work performed

3.1 Individual dynamic measures

The following individual dynamic measures have been extracted.

3.1.1 Long-range temporal correlations (LRTC)

Linear detrended fluctuation analysis (DFA) is used to assess the LRTCs in neuronal oscillations (Hardstone et al., 2012; Peng, Havlin, Stanley, & Goldberger, 1995). The obtained DFA exponent, similar to the Hurst exponent, reflects the self-affinity in narrow-band amplitude fluctuations from a recorded brain region (Eke et al., 2000). We obtained narrow-band amplitude time series, in log-spaced equidistant narrow-band frequencies from 2 to 90 Hz. Filtering was carried out using Morlet wavelets of width parameter $m = 5$. We



used an open-source toolbox named ‘Neurophysiological Biomarker Toolbox (NBT)’ (Peng et al., 1995) to calculate DFA exponents.

3.1.2 Functional excitation-inhibition ratio (fE/I)

The method to calculate fE/I has been recently introduced in (Bruining et al., 2020) and is based on both amplitude fluctuations and spectral power of a given time-series. The steps in the estimation of fE/I are as follows: (1) The wide-band signals were Morlet-filtered into 32 log-equidistant narrowband signals over a bandwidth of 2-90 Hz and their amplitude fluctuations were extracted. (2) Signal profile was formed, i.e., the cumulative sum of demeaned amplitude fluctuation. (3) Signal profile was normalized in each time window (we used fixed a length 40 cycles for each narrow-band signal) by original amplitude, nullifying any influence of original magnitude. (4) Each normalized signal profile window was detrended linearly. (5) Standard deviation for each window was calculated to get windowed-normalized fluctuation function ($W_{nF(t)}$). (6) Mean of original amplitude fluctuation W_{Amp} for each window (same as in step 3) was calculated. (7) Pearson correlation $r(W_{nF(t)}, W_{Amp})$ between the results of step 5 and 6 was calculated, and fE/I was estimated as $1 - r(W_{nF(t)}, W_{Amp})$; ‘1’ representing balanced E/I, ‘< 1’ indicates inhibition dominant and ‘> 1’ is for excitation dominant).

3.2 Inter-areal dynamics

The following functional connectivity (FC) metrics were computed for the MEG full-cohort.

3.2.1 Phase-locking value (PLV)

The PLV is a measure of the phase synchronization between two signals quantifying how their phase differences are preserved during the time course. In the original formulation by (Lachaux, Rodriguez, Martinerie, & Varela, 1999), PLV was defined as:

$$PLV = \frac{1}{N} |\sum_{n=1}^N \exp[i(\varphi_a - \varphi_b)]| \quad (1)$$

where φ_a and φ_b are the phases of the two band-pass filtered signals.

For the current database, the PLV was calculated following the reformulation introduced in (Bruña, Maestú, & Pereda, 2018) (see **Table 3**). PLV was estimated in the classical frequency bands (theta, 4-8 Hz; alpha, 8-12 Hz; beta 1, 12-20 Hz; beta2, 20-30 Hz; beta, 12-30 Hz; gamma, 30-45 Hz) using the epoched data and the beamformer filters provided in **Deliverable 3.5**. The PLV matrices are extracted for parcels given in above-mentioned different atlases, and stored in the files `sub-xxx_task-rest_atlas-{atlas}_PLV.mat`.



3.2.2 Corrected imaginary phase-locking value (ciPLV)

Despite its popularity, the PLV presents an important limitation when used to evaluate FC: its sensitivity to volume conduction and source-leakage effects.

Following the tight relationship of PLV with coherency (the imaginary part of coherency discards zero-lag connectivity and thus is insensitive to volume conduction (Nolte et al., 2004)), it is possible to obtain a PLV-based FC measure that is insensitive to volume conduction. This formulation is known as corrected imaginary PLV (ciPLV) is defined in (Bruña et al., 2018).

For the current database, ciPLV was estimated in the classical frequency bands (theta, 4-8 Hz; alpha, 8-12 Hz; beta 1, 12-20 Hz; beta2, 20-30 Hz; beta, 12-30 Hz; gamma, 30-45 Hz) using the epoched data and the beamformer filters provided in **Deliverable 3.5**. Similar to PLV, ciPLV matrices are extracted following above-mentioned atlases and are stored in the files as: `sub-xxx_task-rest_atlas-{atlas}_ciPLV.mat`.

3.2.3 Weighted phase lag index (wPLI)

Similar to ciPLV, the wPLI (Vinck, Oostenveld, van Wingerden, Battaglia, & Pennartz, 2011) is designed to be insensitive to volume conduction. It takes into account the amplitude of the imaginary component of the cross-spectrum. In this way, relative phases corresponding to a small imaginary cross-spectrum have a lower effect on the corresponding resulting phase synchrony index.

For the current database, wPLI was estimated in the classical frequency bands (theta, 4-8 Hz; alpha, 8-12 Hz; beta 1, 12-20 Hz; beta2, 20-30 Hz; beta, 12-30 Hz; gamma, 30-45 Hz) using the epoched data and the beamformer filters provided in **Deliverable 3.5**. Similar to PLV, wPLI values were averaged following different cortical parcellation templates and are contained in the files `sub-xxx_task-rest_atlas-{atlas}_wPLI.mat`.



Table 3. Summary of the FC measures of phase coupling included in the deliverable.

FC measure	Formulation	Ref.	Parcellation & filenames
Phase-Locking Value (PLV)	$PLV_{ab} = \frac{1}{T} \left \sum_{t=1}^T \dot{x}_{BP,H,a}(t) \cdot (\dot{x}_{BP,H,b}(t))^* \right $ <p>where:</p> $\dot{x}_{BP,H,a}(t) = \frac{x_{BP,H,a}(t)}{ x_{BP,H,a}(t) } = \frac{A(t)e^{i\varphi_a(t)}}{A(t)} = e^{i\varphi_a(t)}$ <p>is the oscillatory part of the analytical band-pass filtered signal.</p>	(Lachaux et al., 1999, Bruña et al., 2018)	AAL sub-xxx_task-rest_atlas-AAL_PLV.mat HO sub-xxx_task-rest_atlas-HO_PLV.mat SCH sub-xxx_task-rest_atlas-schaefer400_PLV.mat
Corrected Imaginary Phase-Locking Value (ciPLV)	$ciPLV_{a,b,t} = \frac{\frac{1}{T} Im[\dot{x}_{a,t} \cdot \dot{x}_{b,t}^T]}{\sqrt{1 - \left(\frac{1}{T} Re[\dot{x}_{a,t} \cdot \dot{x}_{b,t}^T]\right)^2}}$ <p>where $Re[x]$ and $Im[x]$ stand for the real and imaginary parts of x, respectively.</p>	(Bruña et al., 2018)	AAL sub-xxx_task-rest_atlas-AAL_ciPLV.mat HO sub-xxx_task-rest_atlas-HO_ciPLV.mat SCH sub-xxx_task-rest_atlas-schaefer400_ciPLV.mat
Weighted Phase Lag Index (wPLI)	$wPLI = \frac{ Im[X] }{\langle Im[X] \rangle} = \frac{\langle Im[x] \text{ sign } Im[X] \rangle}{\langle Im[X] \rangle}$ <p>where X is the <i>cross-spectrum</i> between the parcel time-series a and b.</p>	(Vinck et al., 2011)	AAL sub-xxx_task-rest_atlas-AAL_wPLI.mat HO sub-xxx_task-rest_atlas-HO_wPLI.mat SCH sub-xxx_task-rest_atlas-schaefer400_wPLI.mat
Long-range temporal correlations (LRTC)		Peng, Havlin, Stanley, & Goldberger, 1995 Palva et al. 2013	SCH sub-xxx_task-rest_atlas-schaefer400_DFA.mat
Functional excitation-inhibition ratio (fE/I)	$f \ E/I = 1 - corr(Amp(T), nF(T))$	Bruining et al., 2020	SCH sub-xxx_task-rest_atlas-schaefer400_fEI.mat
Cross-frequency synchrony (CFS)	$PLV_{CFS,a,b,m} = \frac{1}{N} \left \sum_t \exp [i \cdot (m \cdot \theta_{a,LF} - \theta_{b,HF})] \right $ <p>where $\theta_{a,LF}$ and $\theta_{b,HF}$ are the phases of the parcel time series.</p>	Siebenhühner et al., 2020	SCH sub-xxx_task-rest_atlas-schaefer400_CFS.mat
phase-amplitude coupling (PAC)	$PLV_{PAC,a,b} = \frac{1}{N} \left \sum_t \exp [i \cdot (\theta_{a,LF} - \theta_{b,HF,LF}^{env})] \right $ <p>where $\theta_{b,HF,LF}^{env}$ is the phase of the amplitude envelope of the HF signal filtered with a Morlet filter at LF, and downsampled to match the LF signal's sampling rate. Local PAC was obtained where $a = b$, inter-areal PAC where $a \neq b$.</p>	Siebenhühner et al., 2020	SCH sub-xxx_task-rest_atlas-schaefer400_PAC.mat



3.2.4 Amplitude envelope correlation (AEC)

The envelopes of oscillatory power in the frequency bands of interest were obtained through the absolute value of the analytic signals related to the time-series, and divided into n time epochs of equal length Δt . Finally Pearson correlation coefficient was computed between the envelope time-series within each epoch. The correlation values (one for each epoch) were then averaged across epochs yielding a single average value for each pair of time series (Brookes et al., 2011).

3.2.5 Cross-frequency synchrony (CFS) and phase-amplitude coupling (PAC)

CFS and PAC were computed at frequency ratios $n:m$ from 1:2 to 1:7 for low frequencies in the range 1.2 – 46.9 Hz, and for each parcel-pair p_a, p_b (Siebenhühner et al., 2020) of the Schaefer atlas (17 networks, 400 parcels).

CFS was computed as:

$$PLV_{CFS,a,b,m} = \frac{1}{N} \left| \sum_t \exp [i \cdot (m \cdot \theta_{a,LF} - \theta_{b,HF})] \right| \quad (2)$$

where $\theta_{a,LF}$ and $\theta_{b,HF}$ are the phases of the parcel time series. $\theta_{a,LF}$ was upsampled to match the sampling rate of the HF signal and then ‘phase-accelerated’ by multiplication with m . Local CFS was obtained where $a = b$ and inter-areal CFS where $a \neq b$.

The strength of PAC was quantified with as:

$$PLV_{PAC,a,b} = \frac{1}{N} \left| \sum_t \exp [i \cdot (\theta_{a,LF} - \theta_{b,HF,LF}^{env})] \right| \quad (3)$$

where $\theta_{b,HF,LF}^{env}$ is the phase of the amplitude envelope of the HF signal filtered with a Morlet filter at LF, and downsampled to match the LF signal’s sampling rate. Local PAC was obtained where $a = b$, inter-areal PAC where $a \neq b$.

4. Conclusion

The extracted measures represent a valuable source for the study of neurodegenerative diseases (e.g., unveiling possible disease trajectories), and can be used to optimize and validate computational models of large-scale brain dynamics. The dataset is stored in a dedicated server (<https://vbc.ucm.es/login.php>), arranged using the BIDS standard, to foster interoperability and to address the heterogeneity of data organization.



5. References

- Brookes, M., Hale, J., Zumer, J., Stevenson, C., Francis, S., Barnes, G., ... Nagarajan, S. (2011). Measuring functional connectivity using MEG: methodology and comparison with fcMRI. *NeuroImage*, *56*(3), 1082–1104. <https://doi.org/10.1016/J.NEUROIMAGE.2011.02.054>
- Bruining, H., Hardstone, R., Juarez-Martinez, E. L., Sprengers, J., Avramiea, A.-E., Simpraga, S., ... Linkenkaer-Hansen, K. (2020). Measurement of excitation-inhibition ratio in autism spectrum disorder using critical brain dynamics. *Scientific Reports*, *10*(1), 1–15. <https://doi.org/10.1038/s41598-020-65500-4>
- Bruña, R., Maestú, F., & Pereda, E. (2018). Phase locking value revisited: teaching new tricks to an old dog. *Journal of Neural Engineering*, *15*(5). <https://doi.org/10.1088/1741-2552/AACFE4>
- Desikan, R., Ségonne, F., Fischl, B., Quinn, B., Dickerson, B., Blacker, D., ... Killiany, R. (2006). An automated labeling system for subdividing the human cerebral cortex on MRI scans into gyral based regions of interest. *NeuroImage*, *31*(3), 968–980. <https://doi.org/10.1016/J.NEUROIMAGE.2006.01.021>
- Eke, A., Hermán, P., Bassingthwaighte, J., Raymond, G., Percival, D., Cannon, M., ... Ikrényi, C. (2000). Physiological time series: distinguishing fractal noises from motions. *Pflugers Archiv : European Journal of Physiology*, *439*(4), 403–415. <https://doi.org/10.1007/S004249900135>
- Frazier, J., Chiu, S., Breeze, J., Makris, N., Lange, N., Kennedy, D., ... Biederman, J. (2005). Structural brain magnetic resonance imaging of limbic and thalamic volumes in pediatric bipolar disorder. *The American Journal of Psychiatry*, *162*(7), 1256–1265. <https://doi.org/10.1176/APPI.AJP.162.7.1256>
- Freyer, F., Roberts, J. A., Ritter, P., & Breakspear, M. (2012). A Canonical Model of Multistability and Scale-Invariance in Biological Systems. *PLOS Computational Biology*, *8*(8), e1002634. <https://doi.org/10.1371/JOURNAL.PCBI.1002634>
- Goldstein, J., Seidman, L., Makris, N., Ahern, T., O'Brien, L., Caviness, V., ... Tsuang, M. (2007). Hypothalamic abnormalities in schizophrenia: sex effects and genetic vulnerability. *Biological Psychiatry*, *61*(8), 935–945. <https://doi.org/10.1016/J.BIOPSYCH.2006.06.027>
- Hardstone, R., Poil, S.-S., Schiavone, G., Jansen, R., Nikulin, V. V., Mansvelder, H. D., & Linkenkaer-Hansen, K. (2012). Detrended Fluctuation Analysis: A Scale-Free View on Neuronal Oscillations. *Frontiers in Physiology*, *0*, 450. <https://doi.org/10.3389/FPHYS.2012.00450>
- Lachaux, J. P., Rodriguez, E., Martinerie, J., & Varela, F. J. (1999). Measuring phase synchrony in brain signals. *Human Brain Mapping*, *8*(4)(4), 194–208. [https://doi.org/10.1002/\(SICI\)1097-0193\(1999\)8:4<194::AID-HBM4>3.0.CO;2-C](https://doi.org/10.1002/(SICI)1097-0193(1999)8:4<194::AID-HBM4>3.0.CO;2-C)
- Makris, N., Goldstein, J., Kennedy, D., Hodge, S., Caviness, V., Faraone, S., ... Seidman, L. (2006). Decreased volume of left and total anterior insular lobule in schizophrenia. *Schizophrenia Research*, *83*(2–3), 155–171. <https://doi.org/10.1016/J.SCHRES.2005.11.020>
- Nolte, G., Bai, O., Wheaton, L., Mari, Z., Vorbach, S., & Hallett, M. (2004). Identifying true brain interaction from EEG data using the imaginary part of coherency. *Clinical Neurophysiology*, *115*(10), 2292–2307. <https://doi.org/10.1016/J.CLINPH.2004.04.029>
- Palva, J. M., Zhigalov, A., Hirvonen, J., Korhonen, O., Linkenkaer-Hansen, K., and Palva, S. (2013). Neuronal long-range temporal correlations and avalanche dynamics are correlated with behavioral scaling laws. *Proc. Natl. Acad. Sci. U.S.A.* *110*, 3585–3590. doi: 10.1073/pnas.1216855110.
- Peng, C., Havlin, S., Stanley, H., & Goldberger, A. (1995). Quantification of scaling exponents and crossover phenomena in nonstationary heartbeat time series. *Chaos*, *5*(1), 82–87. <https://doi.org/10.1063/1.166141>
- Roberts, J. A., Boonstra, T. W., & Breakspear, M. (2015). The heavy tail of the human brain. *Current Opinion in Neurobiology*, *31*, 164–172. <https://doi.org/10.1016/J.CONB.2014.10.014>
- Schaefer, A., Kong, R., Gordon, E., Laumann, T., Zuo, X., Holmes, A., ... Yeo, B. (2018). Local-Global Parcellation



- of the Human Cerebral Cortex from Intrinsic Functional Connectivity MRI. *Cerebral Cortex*, 28(9), 3095–3114. <https://doi.org/10.1093/CERCOR/BHX179>
- Siebenhühner, F., Wang, S. H., Arnulfo, G., Lampinen, A., Nobili, L., Palva, J. M., & Palva, S. (2020). Genuine cross-frequency coupling networks in human resting-state electrophysiological recordings. *PLOS Biology*, 18(5), e3000685. <https://doi.org/10.1371/JOURNAL.PBIO.3000685>
- Tzourio-Mazoyer, N., Landeau, B., Papathanassiou, D., Crivello, F., Etard, O., Delcroix, N., ... Joliot, M. (2002). Automated anatomical labeling of activations in SPM using a macroscopic anatomical parcellation of the MNI MRI single-subject brain. *NeuroImage*, 15(1)(1), 273–289. <https://doi.org/10.1006/nimg.2001.0978>
- Vinck, M., Oostenveld, R., van Wingerden, M., Battaglia, F., & Pennartz, C. (2011). An improved index of phase-synchronization for electrophysiological data in the presence of volume-conduction, noise and sample-size bias. *NeuroImage*, 55(4), 1548–1565. <https://doi.org/10.1016/J.NEUROIMAGE.2011.01.055>
- Wit, E., van den Heuvel, E., and Romeijn, J.W. (2012). 'All models are wrong. ': An introduction to model uncertainty. *Stat. Neerl.*